
<https://doi.org/10.15407/ujpe70.2.109>

V.M. ZADOROZHNYI, R.M. BALABAI, O.O. BONDARENKO

Kryvyi Rih State Pedagogical University

(54, Gagarina Ave., Kryvyi Rih 50086, Ukraine;

e-mails: vitaliy_zadorozhniy@ukr.net, balabai@i.ua, alengkagonohova@gmail.com)

PIEZOELECTRIC RESPONSE OF α -FORM POLY(L-LACTIC ACID) TO MECHANICALLY STRESSED STATE

Here, the piezoelectric effects in a polymer (L-lactic acid) under a mechanical action are studied by methods of the density functional theory and first-principles pseudopotential based on own program code. The spatial distributions of the valence electron density, electronic state density, Coulomb potentials in different directions of the PLLA polymer fragment and charge states of its individual atoms are calculated. It is found that only one fragment of the polymer chain allows us to determine the nature of the charge polarization of valence electrons and ions under a mechanical deformation.

Keywords: piezoelectric effects, polymer (L-lactic acid), compression, bending, twisting, density functional theory, first-principle calculations.

1. Introduction

A wide range of materials have been investigated for the piezoelectric energy storage, including inorganic, organic, and composite materials [1]. Piezoelectric polymers are naturally flexible, strong, and easy to be processed, making them favorable for many applications [2]. Piezoelectric polymers such as nylon-11 [3], derived from castor oil; carbon fiber-reinforced polymer [4], and others can successfully replace inorganic ceramic piezoelectrics, which are usually brittle, inflexible and often contain toxic heavy metals – factors that hinder their use in medicine [5]. Piezoelectric polymers can be found in nature. For example, timber is a piezoelectric material due to the presence of cellulose in its structure [6]. Poly(L-lactic acid) (PLLA)

is one of the synthetic biodegradable piezoelectric polymers synthesized by polymerizing L-lactic acid monomers. The piezoelectric functionality of PLLA has been demonstrated as a force sensor in the literature [7]. Despite the fact that these biodegradable piezoelectric materials have lower piezoelectricity than ceramic materials, several approaches can be used to increase their piezoelectricity, for example, by modifying their crystal structures. Zhu and others [8] fabricated a piezoelectric device based on PLLA nanofibers to measure strain and collect piezoelectric energy.

In our work, the piezoelectric effects in a polymer (L-lactic acid) were theoretically investigated using the density functional theory and first-principles pseudopotential methods based on the proprietary software code of Kryvyi Rih State Pedagogical University [9, 10]. The spatial distributions of the valence electron density, electronic state density, Coulomb potentials in different directions of the PLLA polymer fragment, and charge states of its individual atoms are calculated to establish a correlation between the

Citation: Zadorozhnyi V.M., Balabai R.M., Bondarenko O.O. Piezoelectric response of α -form poly(L-lactic acid) to mechanically stressed state. *Ukr. J. Phys.* **70**, No. 2, 109 (2025). <https://doi.org/10.15407/ujpe70.2.109>.

© Publisher PH “Akadempriodyka” of the NAS of Ukraine, 2025. This is an open access article under the CC BY-NC-ND license (<https://creativecommons.org/licenses/by-nc-nd/4.0/>)

ISSN 2071-0194. *Ukr. J. Phys.* 2025. Vol. 70, No. 2

crystal structure and piezoelectric properties, which will allow us to determine its specific application in practice under various mechanical stresses such as compression, bending or twisting.

2. Research Methods and Models

The main value in the formalism of the electron density functional is the charge density. We estimated it from the self-consistent solution of the Kohn–Sham equations for an artificial periodic system:

$$\rho(\mathbf{G}) = \frac{2}{N_T} \sum_{\mathbf{k}} \sum_{\mathbf{j}} \sum_{\alpha \in T} \sum_{\mathbf{G}'} b_j^*(\mathbf{k} + \mathbf{G}' + \alpha\mathbf{G}) \times b_j(\mathbf{k} + \mathbf{G}'), \quad (1)$$

where the index j passed through all occupied states, \mathbf{k} is a vector from the first Brillouin zone, N_T is the number of operators α in the point group T of the atomic basis, and the factor 2 takes the spin degeneracy into account.

The Coulomb potential along a given direction was calculated by the formula, which, in the inverse space, is given by:

$$V_h(\mathbf{G}) = \frac{4\pi e^2 \rho(\mathbf{G})}{G^2}, \quad (2)$$

where $\rho(\mathbf{G})$ is the Fourier component of the electron density (1).

To estimate the redistribution of the electron charge between atoms, the expression in a vicinity of the atom α in the volume V was calculated:

$$q_\alpha = Z_\alpha - \int_{V_\alpha} n(r) d^3. \quad (3)$$

Our calculations were performed under the following conditions: the Brillouin zone summation was replaced by a calculation at a single point, the Gamma point. Self-consistency iterations were terminated if the calculation results of the current iteration coincided with the previous one with a given error. Usually, our results coincided after 5–6 iterations. The number of plane waves in the wave function expansion was reduced by trial calculations. The number of plane waves was chosen to be approximately 20–25 waves per atom of the basis. The atomic basis was not optimized.

In the studied atomic systems, artificial translational symmetry was introduced by constructing a

superlattice with a primitive tetragonal cell and an atomic basis containing complete information about the system under study. The cell was translated in three orthogonal directions. The following objects were developed for the calculations:

Object 1: a single isolated polymer chain fragment (L-lactic acid) of α form, consisting of 45 atoms and oriented within the Laboratory Cartesian coordinate system used in the software package, with its longest side – the carbon framework – along the Z direction. The fragment was subjected to static compression simulation by changing the corresponding atomic coordinates in the direction of the compression force, which is conjugate to the Cartesian Z -direction, i.e., the Z -coordinates of the atoms were reduced to 9% of the initial ones in steps of 2%.

Object 2: one isolated fragment of a polymeric chain (L-lactic acid) of α form, to which the simulation of mechanical impact of the twisting type was applied by the action of the twisting transformation matrix around the Z axis, which depends on the linear angle proportional to the distance of the object point from the fixed point, which was selected in the lowest atom of the polymeric fragment ($\text{angle} = \text{angle}^* Z_i$).

Object 3: a single isolated polymer chain fragment (L-lactic acid) of α form, to which the simulation of mechanical impact of the bending type was applied by the action of the bending transformation matrix around the X -axis. Unlike torsion, in bending deformation, the angle of rotation of a point around the bending axis is proportional to its distance. Bending was performed relative to a fixed point, which was chosen in the center of the polymer fragment.

3. Results and Discussion

We analyzed the changes in the calculated distributions of valence electrons in different regions of the isolated polymer chain fragment (L-lactic acid) α form depending on the mechanical deformation. Figures 1–3 show the spatial distributions of the valence electron density within the entire isolated PLLA fragment at different types and levels of mechanical deformation.

The analysis of just one fragment of the polymer chain already allows us to determine the nature of the redistribution of valence electrons. It can be seen that the electron charge recedes from the hanging ends of the polymer chain and is drawn into the chain (see

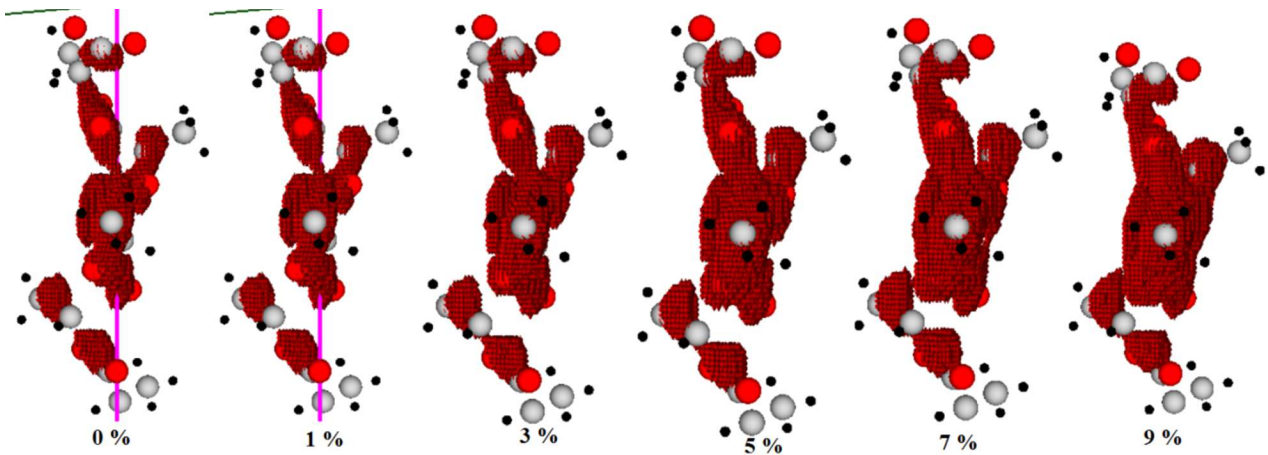


Fig. 1. Spatial distributions of the valence electron density for isovalues (0.9–1.0) of the maximum within a single PLLA chain at different mechanical compression levels

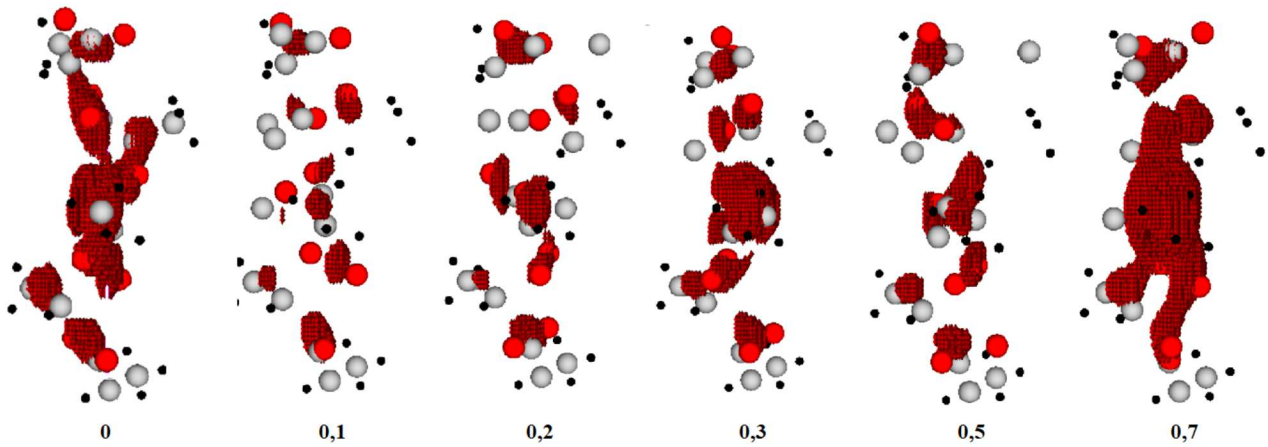


Fig. 2. Spatial distributions of the valence electron density for isovalues (0.9–1.0) of the maximum within a single PLLA chain at different mechanical torsion levels

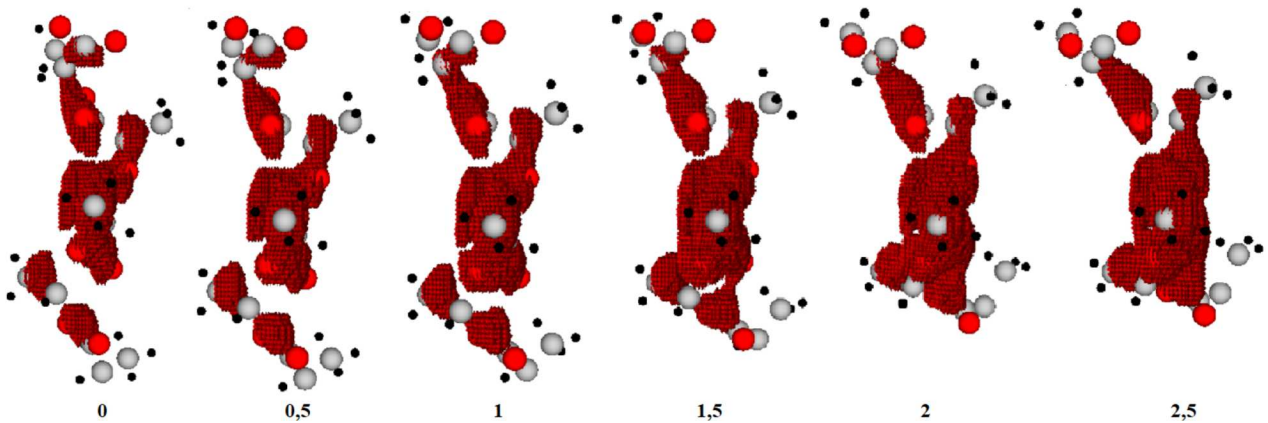
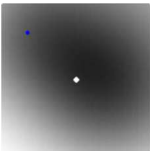
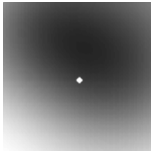
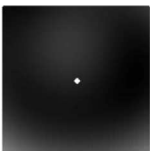
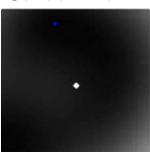
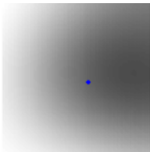
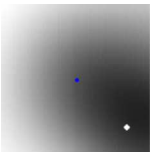
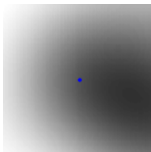
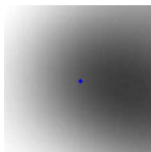
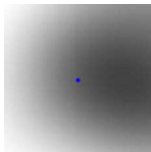
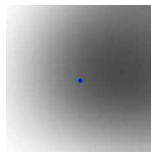
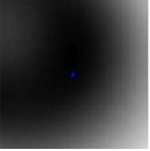
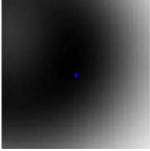
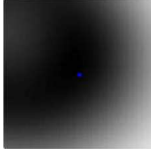
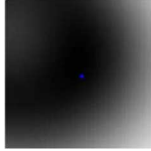
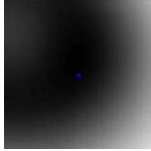
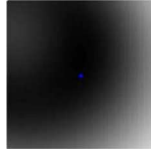
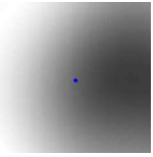
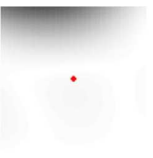
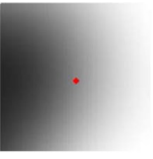
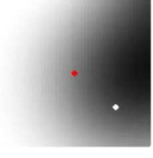
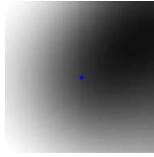
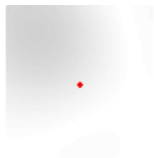
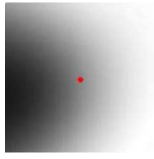
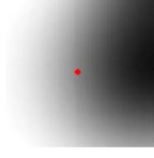
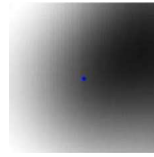
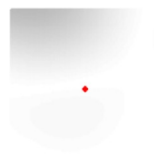
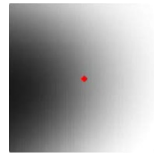
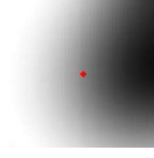
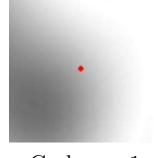
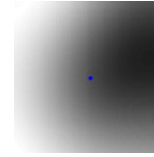
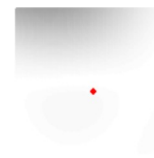
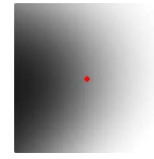
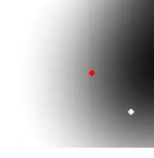
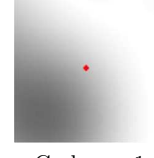
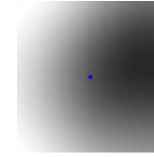
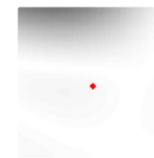
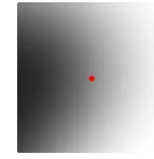
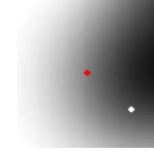
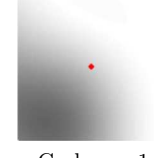
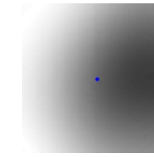
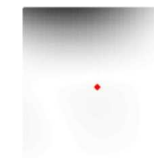
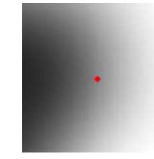
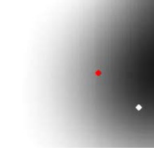


Fig. 3. Spatial distributions of the valence electron density for isovalues (0.9–1.0) of the maximum within a single PLLA chain at different mechanical bending levels

Table 1. Values of electric charges in a vicinity of the C, O, H atoms depending on the polymer bending angle

Bending 0 degrees	Deformation. Bending 0.5 degrees	Deformation. Bending 1 degrees	Deformation. Bending 1.5 degrees	Deformation. Bending 2 degrees	Deformation. Bending 2.5 degrees
Number and type of atom in the centre of the neighbourhood with radius 1.323 Å. Cross-section of the electron density in the neighborhood. Quantity and types of atoms in the neighbourhood. Charge, ee.					
<p>Carbon No. 3</p>  <p>Carbon – 1 Oxygen – 1 2.2110</p>	<p>Carbon No. 3</p>  <p>Carbon – 1 Oxygen – 1 2.7567</p>	<p>Carbon No. 3</p>  <p>Carbon – 1 Oxygen – 1 3.2217</p>	<p>Carbon No. 3</p>  <p>Carbon – 1 Oxygen – 1 3.5569</p>	<p>Carbon No. 3</p>  <p>Carbon – 1 Oxygen – 1 3.8242</p>	<p>Carbon No. 3</p>  <p>Carbon – 1 Oxygen – 1 -2.0043</p>
<p>Carbon No. 9</p>  <p>Carbon – 1 Oxygen – 2 -1.8203</p>	<p>Carbon No. 9</p>  <p>Carbon – 1 Oxygen – 2 -1.8176</p>	<p>Carbon No. 9</p>  <p>Carbon – 1 Oxygen – 2 -1.8117</p>	<p>Carbon No. 9</p>  <p>Carbon – 1 Oxygen – 2 -1.8377</p>	<p>Carbon No. 9</p>  <p>Carbon – 1 Oxygen – 2 -1.8885</p>	<p>Carbon No. 9</p>  <p>Carbon – 1 Oxygen – 1 -1.9211</p>
<p>Carbon No. 12</p>  <p>Carbon – 1 Oxygen – 2 -1.623</p>	<p>Carbon No. 12</p>  <p>Carbon – 1 Oxygen – 2 -1.5677</p>	<p>Carbon No. 12</p>  <p>Carbon – 1 Oxygen – 2 -1.5086</p>	<p>Carbon No. 12</p>  <p>Carbon – 1 Oxygen – 2 -1.424</p>	<p>Carbon No. 12</p>  <p>Carbon – 1 Oxygen – 2 -1.3532</p>	<p>Carbon No. 12</p>  <p>Carbon – 1 Oxygen – 1 -1.2808</p>
<p>Oxygen No. 16</p>  <p>Carbon – 1 Oxygen – 1 4.2634</p>	<p>Oxygen No. 16</p>  <p>Carbon – 1 Oxygen – 1 4.405</p>	<p>Oxygen No. 16</p>  <p>Carbon – 1 Oxygen – 1 4.468</p>	<p>Oxygen No. 16</p>  <p>Carbon – 1 Oxygen – 1 4.6377</p>	<p>Oxygen No. 16</p>  <p>Carbon – 1 Oxygen – 1 4.8323</p>	<p>Oxygen No. 16</p>  <p>Oxygen – 1 0.9557</p>
<p>Oxygen No. 20</p>  <p>Carbon – 1 Oxygen – 1 -0.1385</p>	<p>Oxygen No. 20</p>  <p>Carbon – 1 Oxygen – 1 -0.1884</p>	<p>Oxygen No. 20</p>  <p>Carbon – 1 Oxygen – 1 -0.197</p>	<p>Oxygen No. 20</p>  <p>Carbon – 1 Oxygen – 1 -0.2842</p>	<p>Oxygen No. 20</p>  <p>Carbon – 1 Oxygen – 1 -0.3998</p>	<p>Oxygen No. 20</p>  <p>Carbon – 1 Oxygen – 1 -0.5027</p>

The end of the Table 1

Bending 0 degrees	Deformation. Bending 0.5 degrees	Deformation. Bending 1 degrees	Deformation. Bending 1.5 degrees	Deformation. Bending 2 degrees	Deformation. Bending 2.5 degrees
Number and type of atom in the centre of the neighbourhood with radius 1.323 Å. Cross-section of the electron density in the neighbourhood. Quantity and types of atoms in the neighbourhood. Charge, ee.					
Oxygen No. 24  Carbon - 1 Oxygen - 1 4.0345 Hydrogen No. 26  Carbon - 1 Hydrogen - 1 2.9998 Hydrogen No. 31  Carbon - 2 Hydrogen - 1 4.3965 Hydrogen No. 40  Carbon - 1 Hydrogen - 1 0.6936 Hydrogen No. 45  Carbon - 1 Hydrogen - 1 2.1289	Oxygen No. 24  Carbon - 1 Oxygen - 1 4.2975 Hydrogen No. 26  Carbon - 1 Hydrogen - 1 3.799 Hydrogen No. 31  Carbon - 2 Hydrogen - 1 4.2829 Hydrogen No. 40  Carbon - 1 Hydrogen - 1 0.6675 Hydrogen No. 45  Carbon - 1 Hydrogen - 1 2.132	Oxygen No. 24  Carbon - 1 Oxygen - 1 4.685 Hydrogen No. 26  Carbon - 1 Hydrogen - 1 4.1329 Hydrogen No. 31  Carbon - 2 Hydrogen - 1 4.1905 Hydrogen No. 40  Carbon - 1 Hydrogen - 1 0.7053 Hydrogen No. 45  Carbon - 1 Hydrogen - 1 2.2322	Oxygen No. 24  Carbon - 1 Oxygen - 1 5.0168 Hydrogen No. 26  Carbon - 1 Hydrogen - 1 4.3107 Hydrogen No. 31  Carbon - 2 Hydrogen - 1 4.1871 Hydrogen No. 40  Carbon - 1 Hydrogen - 1 0.7362 Hydrogen No. 45  Carbon - 1 Hydrogen - 1 2.463	Oxygen No. 24  Carbon - 1 Oxygen - 1 5.4178 Hydrogen No. 26  Carbon - 1 Hydrogen - 1 4.4771 Hydrogen No. 31  Carbon - 2 Hydrogen - 1 4.2328 Hydrogen No. 40  Carbon - 1 Hydrogen - 1 0.7717 No. 45  Carbon - 1 Hydrogen - 1 2.8868	Oxygen No. 24  Carbon - 1 Oxygen - 1 5.8538 Hydrogen No. 26  Carbon - 1 Hydrogen - 1 4.5744 Hydrogen No. 31  Carbon - 2 Hydrogen - 1 4.1675 Hydrogen No. 40  Carbon - 1 Hydrogen - 1 0.7987 Hydrogen No. 45  Carbon - 1 -0.6509

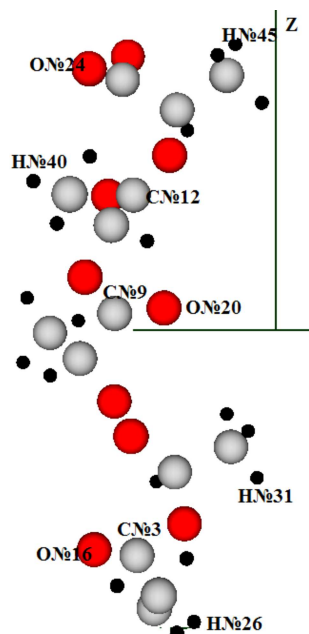


Fig. 4. An isolated fragment of a polymeric chain (L-lactic acid) of α form, consisting of 45 atoms, oriented with its longest side, the carbon framework, along the Z direction of the Laboratory Cartesian coordinate system used in the software package. The atoms in the vicinity of which the electric charges were calculated are marked

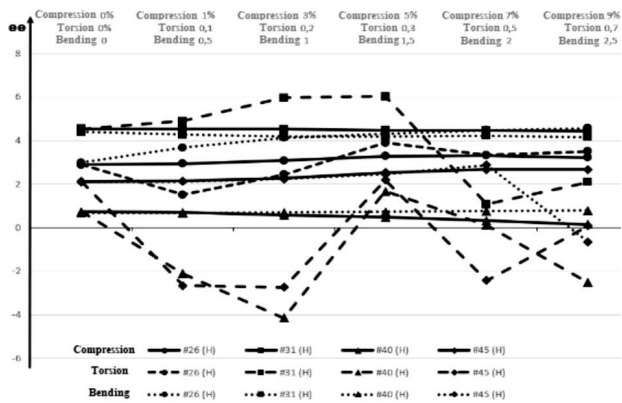


Fig. 5. The values of electric charges in the vicinity of the H atom skeletons depending on the level of compression, torsion, and bending

Figs. 1–3). The mechanical deformation caused additional polarization of dipole components (valence electrons – ionic frameworks), which occur both along the main carbon chain of PLLA and across it.

A more detailed analysis of the redistribution of the density of valence electrons in the polymer under

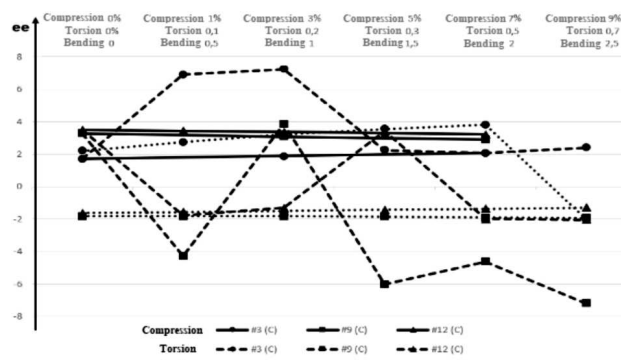


Fig. 6. Values of electric charges in the vicinity of the C atom skeletons depending on the level of compression, torsion, and bending

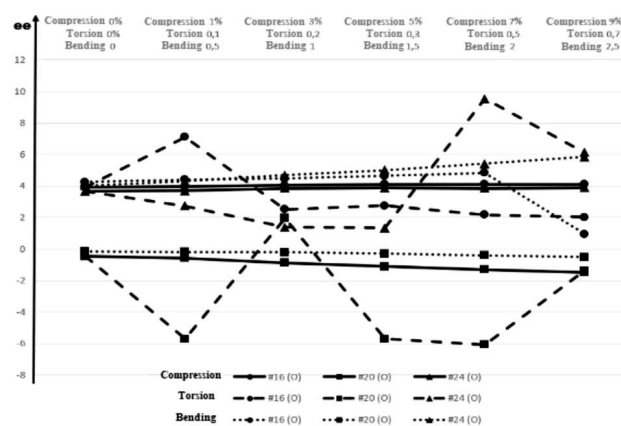


Fig. 7. Values of electric charges in the vicinity of the O atom skeletons depending on the level of compression, torsion, and bending

a deformation was performed. Thus, Figs. 5–7 and, partially, Table 1 show the values of electric charges in a vicinity of the C, O, H atoms of objects 1, 2, and 3, which were estimated by formula (3) in the spherical volume with a radius of 1.323 Å, depending on the level of compression, twisting, and bending, respectively. The atoms for which the charge was calculated are highlighted in Fig. 4 by a signature. The electric charges were calculated in the atomic system of units, in which the charge of an electron is considered equal to one.

The peripheral regions of the polymer chain, which were presented in Table 1 and Fig. 7 by atoms: HNo. 45, ONo. 24, HNo. 26, HNo. 31 and their neighbourhoods with a radius of 1.323 Å, had a “plus” sign of the total charge (negative charge from valence

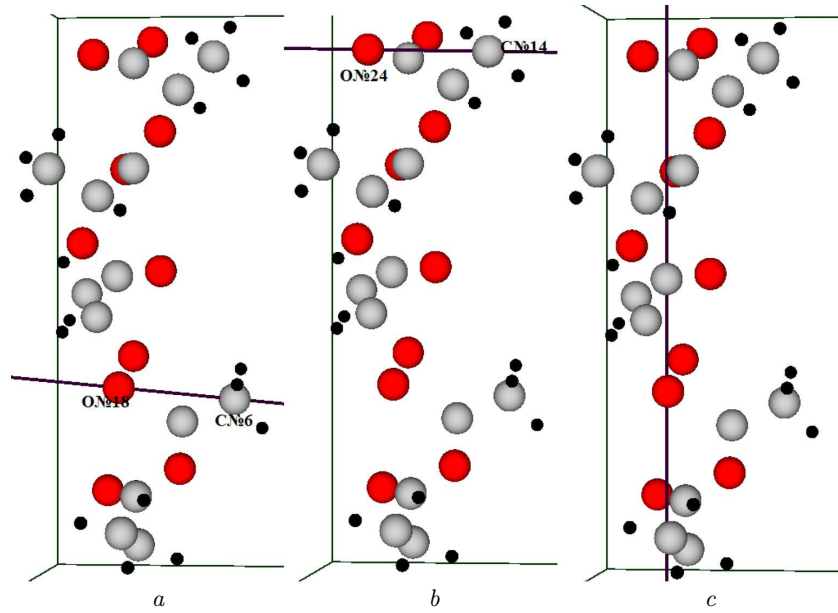


Fig. 8. Directions across (*a*, *b*) and along (*c*) the polymer for calculating Coulomb potential distributions

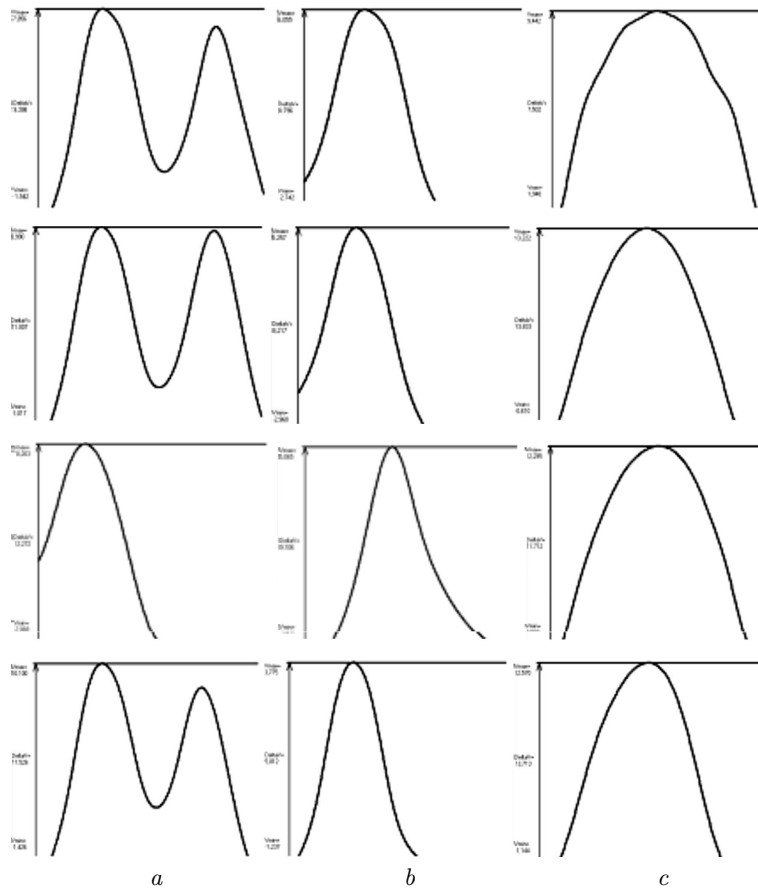


Fig. 9. Distributions of Coulomb potentials in the directions across (*a*, *b*) and along (*c*) the polymer from top to bottom: no deformation, with a compression strain of 9%, torsion by an angle of 0.7, bending by an angle of 2.5

Table 2. Minimum and maximum values in the distributions of Coulomb potentials of valence electrons depending on the polymer strain and the direction of calculation

Direction	Value	Compression, %					
		0	1	3	5	7	9
(a) between CNo. 6 and ONo. 18 atoms	min	-1.426	-1.381	-1.278	-1.178	-1.096	-1.017
	max	9.128	9.219	9.428	9.629	9.812	9.99
(b) between CNo. 14 and ONo. 24 atoms	min	-3.039	-3.037	-3.034	-3.02	-2.994	-2.96
	max	5.494	5.446	5.300	5.241	5.238	5.257
(c) along the polymer	min	0.689	0.509	0.152	-0.163	-0.4	-0.61
	max	12.006	12.151	12.484	12.784	13.014	13.222
Direction	Value	Torsion, %					
		0	0.1	0.2	0.3	0.5	0.7
(a) between CNo. 6 and ONo. 18 atoms	min	-1.426	0.456	-2.156	-3.202	-0.871	-2.069
	max	9.128	9.996	10.185	9.913	9.028	10.203
(b) between CNo. 14 and ONo. 24 atoms	min	-3.039	-3.561	-1.842	-3.612	-3.057	-4.041
	max	5.494	4.972	5.293	5.05	6.191	5.065
(c) along the polymer	min	0.689	0.893	0.788	0.622	0.652	0.583
	max	12.006	11.326	11.906	12.218	11.702	12.295
Direction	Value	Bending					
		0	0.5	1	1.5	2	2.5
(a) between CNo. 6 and ONo. 18 atoms	min	-1.426	-1.503	-1.494	-1.48	-1.443	-1.426
	max	9.128	9.438	9.57	9.698	9.886	10.1
(b) between CNo. 14 and ONo. 24 atoms	min	-2.895	-2.662	-2.304	-1.87	-1.468	-1.237
	max	5.420	5.330	5.158	4.886	4.397	3.775
(c) along the polymer	min	0.290	0.087	-0.147	-0.45	-0.814	-1.144
	max	11.977	12.046	12.125	12.237	12.414	12.57

electrons and positive charge of ions). The middle regions of the polymer chain, which were presented in Table 1 and Fig. 7 by atoms: HNo. 40, ONo. 20, CNo. 12, CNo. 9, ONo. 16, CNo. 3 and their neighbourhoods, had a minus sign of the total charge. Such polarization in the charge distribution increased with an increase in the level of deformation of all studied types. At the same time, the effects of bending and compression along the carbon skeleton of the polymer fibre revealed monotonicity and a low level of charge changes. Whereas, when the polymer was twisted, significant changes in the magnitudes of charges in vicinities of atoms were recorded, even the sign of these total charges changed, which is obviously caused by a significant deformation of chemical covalent bonds.

The distributions of Coulomb potentials in the directions along and across the polymer were calculated using formula (2), which are indicated by lines in Fig. 8.

The numerical values of the extremes in the Coulomb potential distributions are given in Tabl. 2.

A sharper relief of the Coulomb potentials of valence electrons occurs in the direction of the carbon skeleton of the polymer, i.e., along the polymer chain.

4. Conclusions

The spatial distributions of the valence electron density, charges on atoms, and Coulomb potentials for an isolated polymer chain fragment (L-lactic acid) α form were calculated using the density functional theory and ab initio pseudopotentials depending on the

mechanical deformations such as compression, torsion, and bending.

Only one fragment of the polymer chain allows us to determine the nature of the charge polarization of valence electrons and ions under mechanical deformation, namely, the charge departs from the hanging ends of the polymer fragment and retracts into its middle.

An increase in the level of mechanical deformation causes additional polarizations to occur both along the main carbon chain of the polymer and across it.

The effects of bending and compression along the carbon framework of the polymer fibre proved to be more effective than twisting.

A sharper relief of the Coulomb potential of valence electrons occurs in the direction of the polymer carbon framework.

1. N. Sezer, M. Koç. A comprehensive review on the state-of-the-art of piezoelectric energy harvesting. *Nano Energy* **80**, 105567 (2021).
2. M. Smith, S. Kar-Narayan. Piezoelectric polymers: Theory, challenges and opportunities. *International Materials Reviews* **67**, (1), 65 (2022).
3. M. Ali, M.J. Bathaei, L. Beker. Biodegradable piezoelectric polymers: recent advancements in materials and applications. *Adv. Healthcare Mater.* **12**, 2300318 (2023).
4. Ya. Yu, F. Narita. Evaluation of electromechanical properties and conversion efficiency of piezoelectric nanocomposites with Carbon-Fiber-Reinforced polymer electrodes for stress sensing and energy harvesting. *Polymers* **13** (18), 3184 (2021).
5. J. Wu, Y. Fu, G.-H. Hu, S. Wang, C. Xiong. Effect of stretching on crystalline structure, ferroelectric and piezoelectric properties of solution-cast nylon-11 films. *Polymers* **13**, 2037 (2021).
6. J. Sun, H. Guo, G.N. Schädli, K. Tu, S. Schär, F. Schwarze, I. Burgert. Enhanced mechanical energy conversion with

selectively decayed wood. *Sci. Advan.* **7** (11), eabd9138 (2021).

7. E.J. Curry, K. Ke, M.T. Chorsi, K.S. Wrobel, A.N. Miller, A. Patel, I. Kim, J. Feng, L. Yue, Q. Wu, C.L. Kuo, K.W. Lo, C.T. Laurencin, H. Ilies, P.K. Purohit, T.D. Nguyen. Biodegradable piezoelectric force sensor. *Proc. Natl. Acad. Sci. U. S. A.* **115** (5), 909 (2018).
8. J. Zhu, L. Jia, R. Huang. Electrospinning poly(l-lactic acid) piezoelectric ordered porous nanofibers for strain sensing and energy harvesting. *J. Mater. Sci. Mater. Electron.* **28** (16), 12080 (2017).
9. R.M. Balabai, A.G. Solomenko, T.M. Radchenko, V.A. Tarenko. Functionalization of quasi-two-dimensional materials: Chemical and strain-induced modifications. *Progr. Phys. Metals* **23**, 147 (2022).
10. R.M. Balabai, V.M. Zadorozhnyi. Ab initio study of the piezoelectric effects of the 2D semiconductors of IV group monochalcogenides (GeSe, GeS). *Mol. Cryst. Liq. Crystals* **765**, 97 (2023).

Received 27.01.24

V.M. Zadorozhnyi, P.M. Balabai, O.O. Bondarenko

П'ЄЗОЕЛЕКТРИЧНИЙ ВІДГУК
ПОЛІ (L-МОЛОЧНОЇ КИСЛОТИ) α -ФОРМИ
НА МЕХАНІЧНО НАПРУЖЕНИЙ СТАН

У роботі досліджено п'єзоелектричні ефекти в полімері (L-молочна кислота) при механічному впливі методами теорії функціонала густини та псевдопотенціалу на основі власного програмного коду. Розраховано просторові розподіли густини валентних електронів, густини електронних станів, кулонівських потенціалів у різних напрямках фрагмента полімеру PLLA та зарядових станів його окремих атомів. Встановлено, що лише один фрагмент полімерного ланцюга дозволяє визначити характер зарядової поляризації валентних електронів та іонів при механічній деформації.

Ключові слова: п'єзоелектричні ефекти, полімер (L-молочна кислота), стиснення, згинання, скручування, теорія функціонала густини, розрахунки з перших принципів.